Auxiliary donors for phenothiazine sensitizers for dye-sensitized solar cells – how important are they really?†

Audun Formo Buene, [a] Eline Ekornhol Ose,[a] Ane Garborg Zakariassen,[a] Anders Hagfeldt [b] and Bård Helge Hoff *[a]

Auxiliary donors are common design motifs for phenothiazine sensitizers for dye-sensitized solar cells. Despite this, there are only a few reports on their overall contribution to the photon-to-electron conversion efficiency. Twelve sensitizers have been prepared and investigated, including ten different auxiliary donors in addition to a control with no auxiliary donor. The various auxiliary donors improved the PCE by a modest 4–11%, and pyrene (**AFB-19**) was determined to be the most efficient auxiliary donor, with the best cell delivering a PCE of 5.36%. Included in the dye series was also the champion dye within the phenothiazine class. With a reported PCE of 12.1%, it would be an excellent phenothiazine reference dye. The high V_{OC} of 0.83 V of this dye is worth further investigation, but the absorption and photovoltaic performance in this work does not correlate with the previously reported PCE of 12.1%.

Introduction

Dye-sensitized solar cells based on mesoscopic oxide electrodes are a promising third generation photovoltaic technology first described by O'Regan and Grätzel in 1991.[1] Their major advantages over traditional solar cell technologies are their inherent tunability with regard to colour and flexibility. In addition, very low production costs and ease of production are encouraging aspects. Recently, DSSCs have also emerged as interesting components for low power devices for the Internet of Things (IoT).[2] Transparent solid state DSSCs are also a crucial component of a new technology for focus-induced photoresponse distance measurements, which is developed by the company trinamiX.[3]

Dye development has been an important driving force in the DSSC field. The earlier reported dyes were based on chlorophyll-like porphyrin structures[4,5] as well as ruthenium(II) bipyridine complexes such as N3, and later N719.[6] Recognizing the limitations of these dyes led to the development of metal-free dyes, allowing for higher extinction coefficients, tunability and easier purification in dye synthesis.[7] For a more complete description of the workings of a DSSC, dye development and device characterization, we refer the reader to a number of very good reviews on the topics.[8–11]

While metal-based dyes rely on a metal-to-ligand-charge-transfer (MLCT) process, metal-free dyes operate *via* an internal charge transfer excitation and often use a design concept following the donor–π–acceptor/anchor (D–π–A) layout.

Other design concepts without a traditional donor group have also been reported.[12,13] The most utilized anchoring group is cyanoacrylic acid which also provides a pulling effect.[14] Common π-spacers are usually based on phenyls,[15] five-membered heterocycles[16] or fused heterocycles,[17] while popular donor groups include triarylamines,[18] phenothiazines,[19,20] and coumarins,[21] among others.

The role of the donor group is to provide an inductive pushing effect helping with charge injection upon excitation. Donor groups may also be able to carry the positive charge of the sensitizer, keeping them spatially separated from TiO_2 to suppress electron recombination and facilitate regeneration from the redox shuttle. Many metal-free dyes utilize a moiety called an auxiliary donor, making the dye layout a D–D–π–A system, as illustrated in Fig. 1. These auxiliary donors are reported to increase the extinction coefficient of sensitizers when directly in conjugation with the main chromophore, leading to higher power conversion efficiencies of DSSCs.[22]

For the phenothiazine scaffold, some of the most common auxiliary donors are *para*-alkoxy phenyls,[23,24] *ortho*- and *para*-alkoxy phenyls,[20,25] triphenylamines[26,27] and carbazoles.[28]

Although a number of auxiliary donors have been tested for the phenothiazine scaffold, only a few reports actually compared the auxiliary donors to the auxiliary donor-free dye.[24,29,30] In these cases the contribution from the auxiliary donors varies from a 16% decrease to a 14% increase in performance, thus highlighting the importance of understanding how different

[a]*Department of Chemistry, Norwegian University of Science and Technology (NTNU), N-7491 Trondheim, Norway. E-mail: bard.h.hoff@ntnu.no*

[b]*Laboratory of Photomolecular Science, Institute of Chemical Sciences and Engineering, École Polytechnique Fédérale de Lausanne (EPFL), Chemin des Alambics, Station 6, CH-1015 Lausanne, Switzerland*

† Electronic supplementary information (ESI) available. See DOI: 10.1039/c9ta00472f

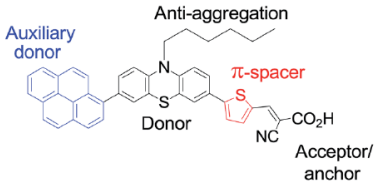

Fig. 1 D–D–π–A structure of AFB-19.

auxiliary donors affect the phenothiazine dye performance. Because the aromatic system of 10*H*-phenothiazine in the ground state is bent, the conjugation is broken at the N and S bridges. This implies that the nature of the auxiliary donor is predominantly to provide an inductive push in the push–pull system of D–D–π–A phenothiazine dyes.

However, the auxiliary donor is also part of the sensitizer molecule that is most likely to interact with the redox shuttle in regeneration of the oxidized dye molecule. Therefore, the role of the auxiliary donor must be more complex than that of a simple electron donating substituent. Several auxiliary donors have been designed to increase its interactions with certain redox shuttles, in particular copper and cobalt complexes.[31–33]

In order to gain further understanding of the role and importance of the auxiliary donor in phenothiazine dyes, we have prepared ten dyes by varying only the auxiliary donor. The rest of the dye molecules remain the same with a thiophene π-spacer, *n*-hexyl anti-aggregation chain, 10*H*-phenothiazine core and cyanoacrylic acceptor and anchoring group. The auxiliary donors selected for this study include six different phenyl-based, three naphthyl-based and pyrene, as shown in Fig. 2. In addition we have included a dye without any auxiliary donor, which was previously reported by both Yang *et al.*[34] and Wei *et al.*[35]. Finally, a reference dye reported by Nagarajan *et al.*[36] was also synthesized in an attempt to verify their claim of over 12% efficiency, which was also used as a helpful yardstick for our own sensitizers.

Results and discussion

Dye synthesis

The synthesis of the building block 3,7-dibromo-10-hexyl-10*H*-phenothiazine (**1**) as well as dyes **AFB-8** and **AFB-9** has previously been reported by the authors.[37] All detailed synthetic procedures are given in the ESI,† and a general synthesis scheme for dyes **AFB-8**, **9**, and **12–19** is shown in Scheme 1. The various auxiliary donors were introduced using a Suzuki cross coupling from their respective aryl boronic acids. This reaction displays low chemoselectivity, leading to roughly a 1 : 2 : 1 distribution of starting material **1**, the desired monocoupled products and the dicoupled byproducts. The starting material is possible to recover, and the purifications are usually uncomplicated, so we have selected this approach rather than the fairly popular route of a monobromination followed by a Suzuki coupling and then another bromination.[24,25] If no π-spacer is required, then formylation followed by bromination is a common approach.[23,38] In the synthesis of dye **18**, the *tert*-butyldimethylsilyl ether (TBDMS) protecting group of the naphtholic boronic acid was cleaved during the Suzuki coupling, and rather conveniently the deprotected naphthol product **8** was obtained. Deprotection of TBDMS with mild carbonate bases or palladium(II) is not unheard of,[39,40] but we were positively surprised by the efficiency of the deprotection, eliminating the need for a separate deprotection step.

In order to efficiently introduce the thiophene π-spacer, a borylation-Suzuki two-step approach was used. First the building blocks with the auxiliary donor moieties were borylated, following a protocol by Billingsley and Buchwald.[41] Without further purification, the crude phenothiazine pinacol boronic esters were coupled with 5-bromo-2-thiophenecarboxaldehyde using $Pd(OAc)_2$ and SPhos in a 1 : 1 (v/v) mixture of water and 1,4-dioxane at 80 °C. The resulting aldehydes were then converted into cyanoacrylic acid anchoring groups *via* the Knoevenagel condensation following the procedure of Iqbal *et al.*[42] using

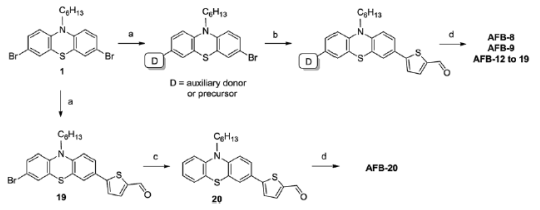

Scheme 1 General synthesis route to dyes AFB-8, 9, and 12–19 as well as the dehalogenation route to AFB-20. (a) Suzuki coupling, (b) borylation-Suzuki two-step reaction, (c) Pd-catalyzed dehalogenation, and (d) Knoevenagel condensation. For details, see the ESI.†

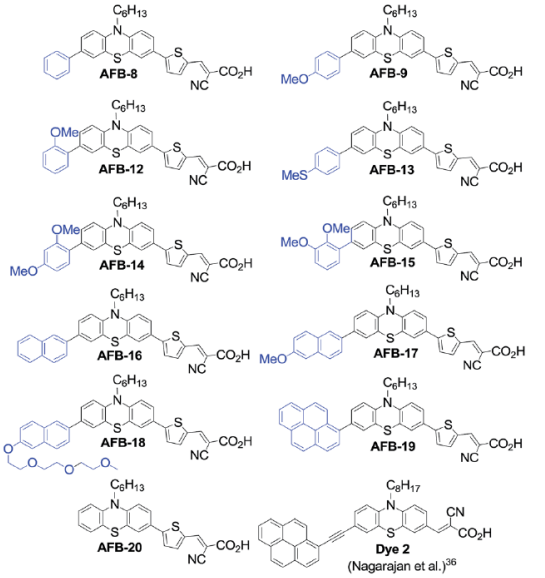

Fig. 2 Structures of the twelve dyes investigated.

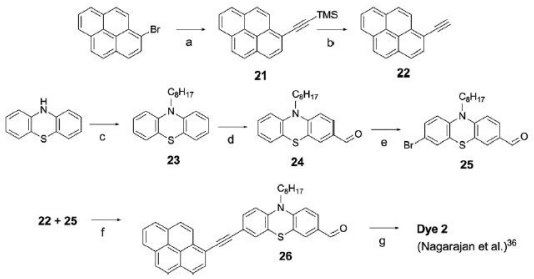

Scheme 2 Synthetic route to Dye 2. (a) Ethynyltrimethylsilane, $PdCl_2(PPh_3)_2$, CuI, Et_3N, 80 °C; (b) NaOH, r.t.; (c) NaH, 1-bromooctane, 66 °C; (d) DMF, $POCl_3$, 1,2-dichloroethane, reflux; (e) NBS, r.t.; (f) $PdCl_2(PPh_3)_2$, CuI, Et_3N, 80 °C; (g) cyanoacetic acid, piperidine, 80 °C.

cyanoacetic acid and piperidine in acetonitrile. The workup and purification conditions were kept as similar as possible for all the target molecules, in case any residual reagents or solvents affected the molecular properties in any way.

Sensitizer **AFB-20** has previously been prepared through monobromination approaches by Yang *et al.*[34] and Wei *et al.*[35] By using the precursors already at hand, we obtained **AFB-20** through another route (Scheme 1). First, a Suzuki coupling catalyzed by the $Pd(OAc)_2$/SPhos system introduced the thiophene carboxaldehyde in a non-selective manner. (5-Formylthiophen-2-yl)boronic acid proved to be less stable than phenyl-based boronic acids; thus, a larger excess (1.5 eq.) was required to obtain comparable conversion.

The monocoupled product **19** obtained after purification was debrominated in a palladium catalyzed reaction as reported by Chen *et al.*,[43] using $Pd(OAc)_2$, triphenylphosphine and K_2CO_3 in *n*-butanol at 100 °C to yield compound **20**. The Knoevenagel condensation produced sensitizer **AFB-20**, bearing no auxiliary donor.

Because the reference sensitizer **Dye 2** has no π-spacer between the phenothiazine core and the anchoring group, a slightly different synthetic route had to be employed (see Scheme 2). First, 10*H*-phenothiazine was alkylated at the 10*H* nitrogen atom, followed by monoformylation by Vilsmeier–Haack reaction and a bromination with *N*-bromosuccinimide (NBS). The resulting building block **25** was then coupled with 1-ethynylpyrene (**22**) in a Sonogashira cross coupling before the final Knoevenagel reaction installed the anchoring group using the same conditions as for the other dyes.

Photophysical properties

The UV/Vis absorption spectra of all dyes in THF and anchored on TiO_2 films are shown in Fig. 3, and extinction coefficients and absorption maxima are given in Table 1. The absorption spectra of all dyes display two major peaks: one between 300 and 400 nm is attributed to the π–π* excitation of the aromatic system, while the other peak is found in the region between 400 and 500 nm, which is the internal charge transfer (ICT)

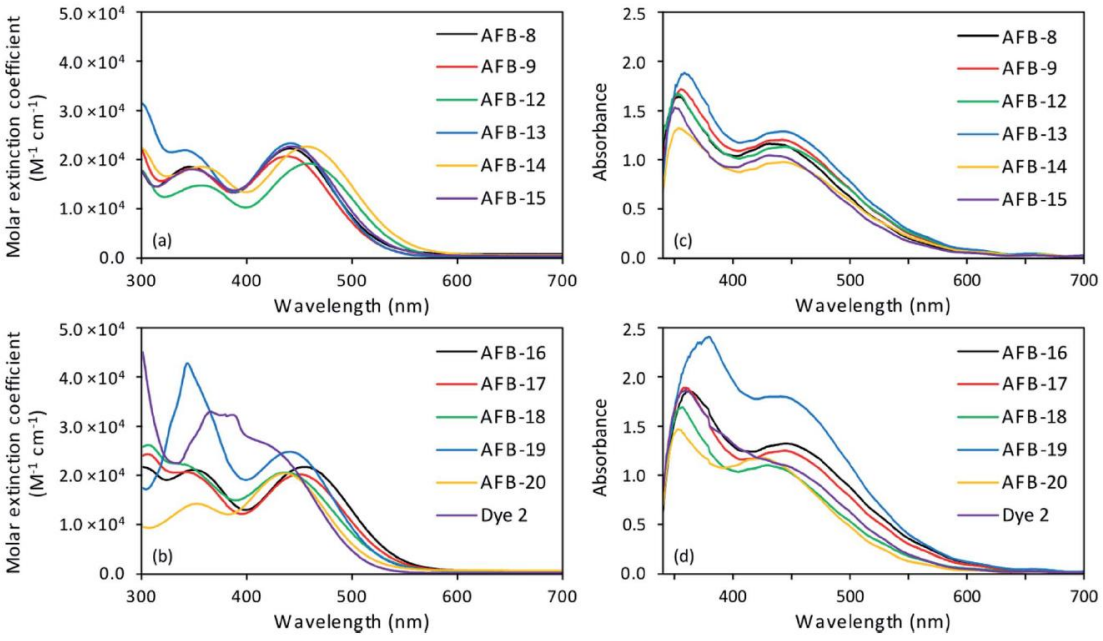

Fig. 3 (a and b) Absorption spectra of all dyes in THF solution (2×10^{-5} M). (a) AFB-8, 9, and 12 to 15 have phenyl-based donors, (b) AFB-16 to 18 have naphthyl-based donors, and AFB-19 and Dye 2 have pyrene donors. Dye AFB-20 has no auxiliary donor. (c and d) Absorption spectra of all dyes on TiO_2 films (2.5 μm, 18NR-T, GreatcellSolar).

Table 1 Photophysical properties of all dyes

Dye	λ_{abs}[a] (nm)	ε (M^{-1} cm^{-1})	Em.[b] (nm)	λ_{abs}[c] on TiO_2 (nm)	$E_{0\text{-}0}$[d] (V)	E_{ox}[e] (V *vs.* SHE)	E_{LUMO}[f] (V *vs.* SHE)
AFB-8	441	22 200	626	432	2.32	0.94	−1.38
AFB-9	439	20 600	637	441	2.33	0.90	−1.43
AFB-12	459	19 050	601	444	2.36	0.91	−1.45
AFB-13	442	23 250	629	443	2.32	0.92	−1.40
AFB-14	457	22 600	618	444	2.32	0.87	−1.45
AFB-15	443	22 600	617	431	2.36	0.86	−1.50
AFB-16	455	21 350	618	445	2.34	0.93	−1.41
AFB-17	450	19 850	629	440	2.30	0.90	−1.40
AFB-18	437	20 200	594	430	2.32	0.90	−1.42
AFB-19	441	24 450	620	441	2.36	0.92	−1.44
AFB-20	436	20 050	624	426	2.36	1.01	−1.35
Dye 2	418	27 550	585	n/a[g]	2.42	1.06	−1.36

[a] Maximum of the most red-shifted peak. [b] Emission when the ICT band is excited, in THF solution. [c] Maximum of the most red-shifted peak on TiO_2 (2.5 μm, GreatcellSolar 18NR-T). [d] Calculated from the intersection of the absorption and normalized emission spectra. [e] Measured in DMF *vs.* Fc^+/Fc and converted to V *vs.* SHE by a conversion factor of 0.624. [f] Calculated from $E_{ox} - E_{0\text{-}0}$. [g] No clear peak to assign.

transition process. The ICT peaks of dyes on TiO_2 are blue-shifted by approximately 10 nm compared to the solution measurements. The absorption of the two pyrene-containing sensitizers displays irregular features in the spectra, likely to stem from separate absorptions within the pyrene moiety. The UV/Vis absorption spectra of 1-bromopyrene and 1-ethynylpyrene (ESI, Fig. S2†) display similar irregular absorption features in the same region.

All the sensitizers with phenyl-based auxiliary donors have very similar UV/Vis absorption properties. The absorption maxima of the two dyes with *ortho*-methoxy substituents on the phenyl donor are red-shifted by about 20 nm compared to the rest of the selection. However, the optical bandgaps are all in the range of 2.32–2.36 eV, and the differences in extinction coefficients are also very small. The naphthyl series displays largely the same properties as the phenyl dyes in terms of bandgaps, absorption maxima and extinction coefficients. For this series, the triethylene oxide methyl ether containing dye **AFB-18** causes a blue-shift of the absorption maxima of about 15 nm; however, the bandgaps are virtually unchanged. The spectrum of **AFB-20** (no auxiliary donor) reveals an ICT band comparable in intensity and position to that of the dyes with auxiliary donors, but the π–π* excitation is noticeably less pronounced. From UV/Vis absorption spectra it is therefore quite clear that the auxiliary donors in phenothiazine dyes do not significantly increase the ICT transition.

Electrochemical properties

Cyclic voltammetry was performed for all dyes to determine the oxidation potentials of the sensitizers, and they all displayed a single reversible oxidation peak. The dyes are sparingly soluble in acetonitrile, so DMF was selected to ensure that all dyes could be measured in the same solvent. Acetonitrile is the main component of the DSSC electrolyte, so when measuring

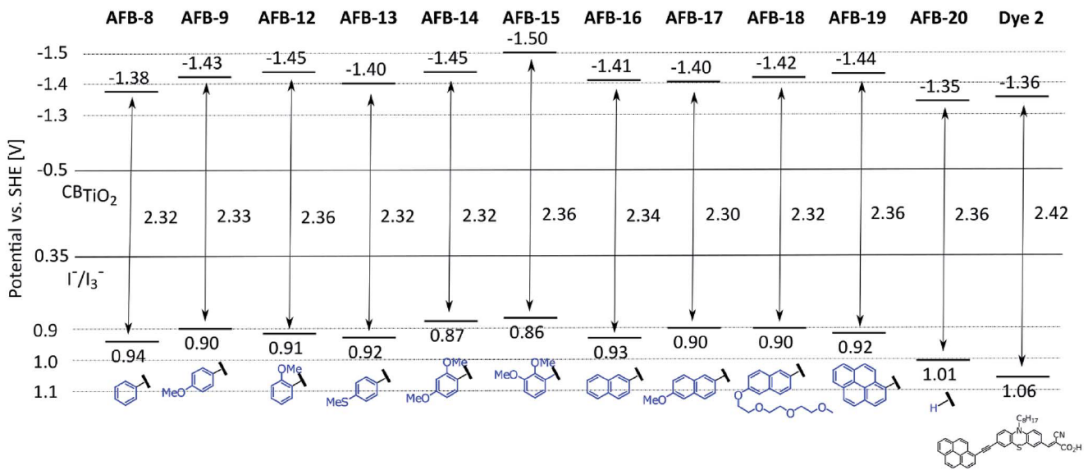

Fig. 4 HOMO and LUMO levels of all dyes. We calculated the HOMO levels from the oxidation potentials of the dyes measured with cyclic voltammetry, and the LUMO levels were calculated from the optical band gaps.

the sensitizers in DMF slightly shifted values may be obtained, but any difference is assumed to be comparable for all twelve sensitizers and not of significant magnitude.[44] Cyclic voltammograms are shown in the ESI (Fig. S3 and S4†), the extracted values for the oxidation potentials *vs.* SHE are shown in Table 1, and Fig. 4 gives a visual summary of the position of the HOMO and LUMO levels of the dyes. All the dyes apart from **AFB-20** and **Dye 2** display an E_{ox} value in the range of 0.86–0.94 V *vs.* SHE. For **AFB-20** and **Dye 2**, the E_{ox} values were found to be 1.01 and 1.06 V, respectively. Compared to **AFB-20**, the introduction of these auxiliary donors raises the HOMO levels by up to 0.15 eV. While using the I^-/I_3^- redox couple there is still sufficient driving force for regeneration, a higher HOMO could give rise to regeneration problems when working with cobalt or copper redox couples. The di-substituted auxiliary donor dyes (**AFB-14** and **15**) have, by a very small margin, the highest positioned HOMO levels. Only slightly below are the mono-substituted phenyl and naphthyl-substituted dyes, which are indistinguishable by cyclic voltammetry.

All the oxidation potentials should be sufficiently higher than the redox potential of the I^-/I_3^- electrolyte (0.35 V *vs.* NHE[45]) in order for efficient regeneration to take place. The calculated LUMO levels of the dyes ($E_{ox} - E_{0\text{–}0}$) are all found from −1.35 to −1.50 V *vs.* SHE, giving all sensitizers sufficient driving force for the charge injection process into TiO_2 (−0.5 V *vs.* SHE) to be favorable.

Photovoltaic performance

Three DSSC devices were fabricated and characterized for each sensitizer. The *J*–*V* curves measured under 1 sun AM 1.5G illumination (100 mW cm^{-2}) and the incident-photon-to-current conversion efficiency (IPCE) spectra are shown in Fig. 5 and 6, respectively. When comparing **AFB-20** to the rest of the dyes, it is clear that the use of an auxiliary donor improves the PCE by 4–11%, with an average improvement of 7% (Table 2). The most efficient dyes, **Dye 2** and **AFB-19**, also display a higher dye loading compared to **AFB-20** (ESI, Table S1†). By grouping the efficiencies of the phenyl-based (**AFB-8**, **9**, and **12–15**), naphthyl-based (**AFB-16**, **17**, and **18**) and pyrene (**AFB-19**) auxiliary donors, the average PCE values are 4.80, 4.86 and 5.00%, respectively. The series composed of **AFB-8**, **AFB-16** and **AFB-19** also displays the same trend. The efficiencies increase from 4.76% for phenyl to 4.90% for naphthyl and 5.00% for the pyrene auxiliary donor. We must however stress that the statistical basis for these claims is marginal, as the overall performance differences between the auxiliary donors are relatively small.

From the IPCE spectra in Fig. 6 it is clear that **Dye 2** is an efficient light harvesting molecule but has the narrowest IPCE

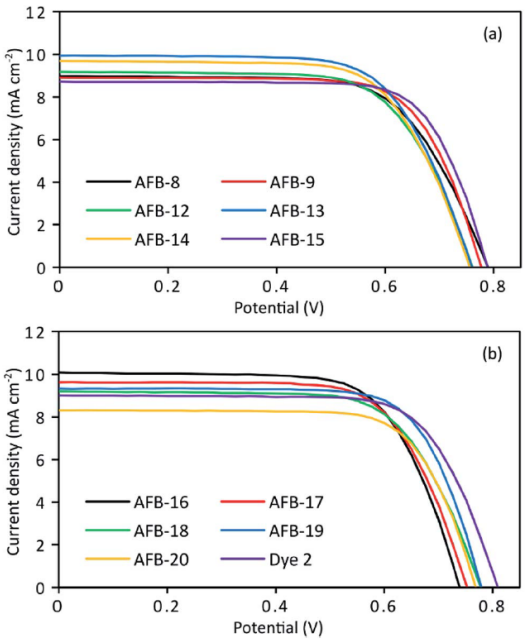

Fig. 5 Current–voltage plots for the best DSSC device fabricated for each sensitizer.

Table 2 Photovoltaic performance of all dyes under 1 sun AM 1.5G illumination and from IPCE measurements

Dye	IPCE J_{SC}[a] (mA cm^{-2})	J_{SC} (mA cm^{-2})	V_{OC} (V)	FF	PCE (%)
AFB-8	8.76	9.12 ± 0.15	0.78 ± 0.01	0.67 ± 0.00	4.76 ± 0.00
AFB-9	8.73	8.89 ± 0.07	0.78 ± 0.00	0.70 ± 0.02	4.81 ± 0.13
AFB-12[b]	8.84	9.03 ± 0.21	0.75 ± 0.01	0.69 ± 0.01	4.67 ± 0.10
AFB-13	9.28	9.40 ± 0.48	0.76 ± 0.00	0.70 ± 0.02	4.95 ± 0.15
AFB-14	9.49	9.32 ± 0.32	0.75 ± 0.00	0.68 ± 0.00	4.76 ± 0.19
AFB-15	8.62	8.65 ± 0.07	0.79 ± 0.00	0.71 ± 0.02	4.84 ± 0.19
AFB-16	10.02	9.90 ± 0.30	0.73 ± 0.01	0.68 ± 0.01	4.90 ± 0.17
AFB-17	9.47	9.46 ± 0.14	0.74 ± 0.00	0.70 ± 0.01	4.90 ± 0.14
AFB-18	8.91	8.75 ± 0.45	0.78 ± 0.00	0.70 ± 0.02	4.79 ± 0.11
AFB-19	9.16	9.00 ± 0.44	0.78 ± 0.00	0.72 ± 0.02	5.00 ± 0.20
AFB-20	7.97	8.21 ± 0.05	0.76 ± 0.00	0.72 ± 0.01	4.51 ± 0.08
Dye 2	8.55	8.91 ± 0.07	0.83 ± 0.01	0.70 ± 0.02	5.16 ± 0.03
N719	12.97	13.20 ± 0.13	0.76 ± 0.01	0.70 ± 0.01	6.98 ± 0.10

[a] Obtained by integration of the IPCE spectrum over the 1 sun AM 1.5 G spectrum. [b] Average values of two cells.

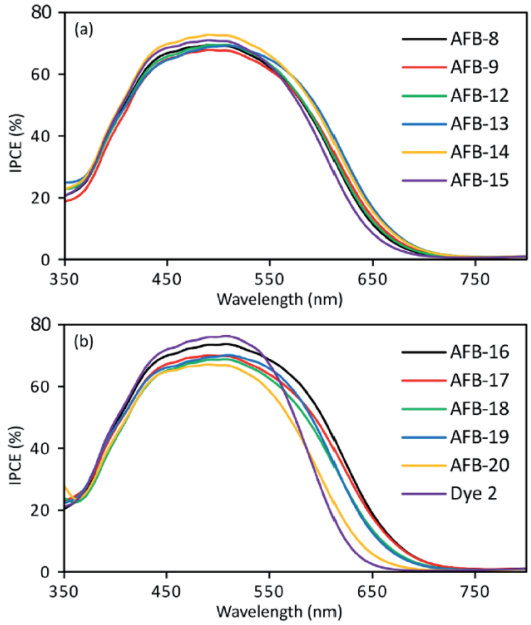

Fig. 6 IPCE spectra for the best DSSC device fabricated for each sensitizer.

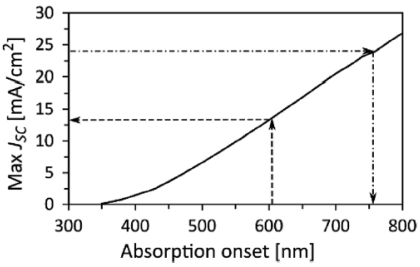

Fig. 7 By integration of the AM 1.5G solar spectrum the theoretical maximum J_{SC} attainable from a device can be calculated and plotted against the corresponding sensitizer absorption onset.[46] The arrows indicate the maximum J_{SC} for a dye with an absorption onset of 605 nm and the required onset to achieve a J_{SC} of 24 mA cm^{-2}.

spectrum of the dyes in this study. The no auxiliary donor dye **AFB-20** also suffers from lower absorption in the region above 500 nm, resulting in a lower overall performance. Not surprisingly, the rest of the sensitizers have very similar IPCE spectra.

The sensitizer **Dye 2** is previously characterized with an impressive J_{SC} of 24.2 mA cm^{-2} and V_{OC} of 846 mV.[36] By the addition of 50 eq. of chenodeoxycholic acid (CDCA) to the staining solutions, the authors reported a 6% decrease in dye loading from 5.51×10^{-7} to 5.20×10^{-7} mol cm^{-2}, J_{SC} increased by 77% and the PCE was improved by 62%. From Fig. 7, it is evident that a sensitizer delivering this impressive J_{SC} will need an absorption onset above 760 nm, corresponding to a bandgap smaller than 1.63 eV.[46] In addition, integration of the IPCE spectra published by Nagarajan *et al.*[36] yields a more modest 7 mA cm^{-2}, and an absorption onset of 605 nm estimated from the published absorption spectra on TiO_2 supports a maximum short-circuit current of 13 mA cm^{-2}. The reported open-circuit voltage is also remarkably high, considering the reported electrolyte contains 0.5 M LiI. The presence of LiI in the electrolyte reduced the V_{OC} by lowering the Fermi level of TiO_2, and the V_{OC} obtained for the same sensitizer in this work was 830 mV without any addition of LiI. Based on the insufficient absorption properties, the lack of a reference sensitizer and the inconsistencies between the published IPCE and *J–V* data, it is the authors' opinion that a calibration error or similar is the cause of the 12.1% PCE reported by Nagarajan *et al.* As stated by Christians *et al.*[47] for the field of perovskite solar cells, any difference larger than 20% between J_{SC} values from *J–V* sweeps under 1 sun and J_{SC} from IPCE integration should call for further experimental support or explanation. There should be no reason for this not to be considered the best practice within the DSSC field as well.

The best sensitizer, **AFB-19**, was also tested with the copper electrolyte, $Cu^{(II/I)}(tmby)_2TFSI_{2/1}$. The devices were fabricated using photoanodes with 4 μm 30NR-D TiO_2 paste + 4 μm scattering paste, and counter electrodes with a catalytic PEDOT layer deposited by electropolymerization.[48] A moderate PCE of 2.27% was obtained for the devices. The *J–V* spectra and data are given in the ESI (Fig. S5 and Table S2†). The performance was likely affected by the HOMO level position of **AFB-19**, only 50 mV below the redox potential of the Cu(tmby) electrolyte reported at 0.87 V.[49] Photovoltages of up to 1.1 V are common for this electrolyte,[50] but our devices delivered a V_{OC} of only 910 mV, indicating that an insufficient driving force for the dye regeneration could be the issue. A solution could be to change to a redox couple with a more negative oxidation potential, as shown by El-Shishtawy *et al.* for similar compounds with a cobalt (II/III) electrolyte.[51]

The best dye from the preliminary screening with the iodide electrolyte was **AFB-19**. As pyrenes are prone to π-stacking[52] and as our best sensitizer had the pyrene auxiliary donor, we were eager to see how dependent the performance was on the presence of the anti-aggregation additive chenodeoxycholic acid (CDCA) in the staining solutions. Five new sets of devices were fabricated with zero, 1, 5, 10 and 20 molar equivalents of CDCA (relative to the sensitizer) in the staining solution, corresponding to 0, 0.5, 2.5, 5 and 10 mM CDCA. All other variables were unchanged from the initial efficiency screening, and the results are summarized in Table 3 and Fig. 8. As shown, no addition of CDCA yields the lowest J_{SC} and affects the fill factor negatively. We have no other explanation for this behavior than the undesirable intermolecular π–π interactions between adjacent sensitizers. The V_{OC} varies by only 11 mV over the entire concentration range, meaning that the conduction band edge of TiO_2 is not affected, nor the injected electron density. The J_{SC} is a crucial variable to the differences in PCE, and a slight drop in J_{SC} is observed with increasing the amount of CDCA from 10 to 20 equivalents, resulting in the peak PCE to be found at 10 equivalents. The peak PCE value for **AFB-19** in this

Table 3 CDCA optimization study for sensitizer AFB-19. The concentrations of CDCA in the staining solutions were 0, 0.5, 2.5, 5.0 and 10.0 mM. The results are averages of three cells

CDCA (eq.)	CDCA conc. (mM)	J_{sc} (mA cm^{-2})	V_{oc} (mV)	FF	PCE (%)
0	0	8.11 ± 0.16	758 ± 6.9	0.67 ± 0.01	4.12 ± 0.07
1	0.5	8.59 ± 0.23	763 ± 9.4	0.70 ± 0.02	4.61 ± 0.21
5	2.5	9.16 ± 0.08	753 ± 4.5	0.70 ± 0.01	4.82 ± 0.11
10	5.0	9.73 ± 0.23	764 ± 6.0	0.71 ± 0.01	5.25 ± 0.11
20	10.0	9.66 ± 0.09	758 ± 7.8	0.70 ± 0.01	5.14 ± 0.04

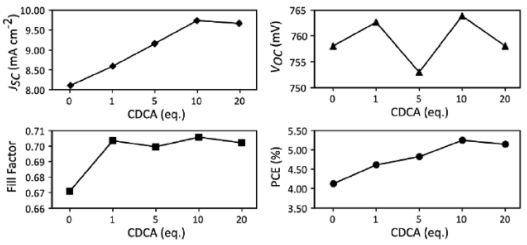

Fig. 8 DSSC characteristics for various CDCA concentrations ranging from zero to 20 equivalents for sensitizer AFB-19. Average values from three devices.

concentration screening was 5.25% with a smaller standard deviation compared to the same series in the preliminary screening, corresponding to a 27% increase in performance compared to 0 mM CDCA. As the other auxiliary donors are considered less prone to aggregation, lower concentrations of CDCA could be favorable, but further investigation would be needed for each sensitizer.

In order to explain the high V_{OC} observed for **Dye 2** we conducted electron lifetime and charge extraction experiments on a new set of devices. Also included were the most (**AFB-19**) and least (**AFB-12**) efficient dyes of the study in addition to the no auxiliary donor dye (**AFB-20**).

The V_{OC} of a device is normally dictated by the position of the TiO_2 Fermi level and the redox potential of the redox couple. Further, the Fermi level position of the TiO_2 is in turn dependent on both the conduction band edge and the electron concentration. From charge extraction measurements at different light intensities, one obtains a range of extracted charges with corresponding open circuit potentials. By comparing the lines from the sensitizers in Fig. 9a at the same charge density, it is possible to estimate the relative conduction band shift caused by each sensitizer from the horizontal shift of each line. Consequently, the conduction band edge of **Dye 2** is shifted upwards by 45 mV relative to that of **AFB-12**.

By correcting the V_{OC} values by the conduction band edge shift observed in Fig. 9a, a new set of lifetime curves can be obtained. By exponential regression, the lifetime values for the potentials of the charge extraction measurements can be calculated. Finally, by plotting the calculated lifetimes against the Q_{OC} values one is able to compare the lifetime measurements of the sensitizers at the same electron density (see Fig. 9b).[53]

The effect of the auxiliary donor on the lifetime can be seen when comparing **AFB-20** to **AFB-12**. The presence of the 2-methoxyphenyl auxiliary donor in **AFB-12** doubles the lifetime compared to **AFB-20**, meaning that the recombination is slowed down by the introduction of the auxiliary donors. This could be highly useful if other redox couples more prone to recombination are of interest for similar sensitizers. Because the lifetime of **Dye 2** is similar to that of both **AFB-12** and **AFB-19**, we

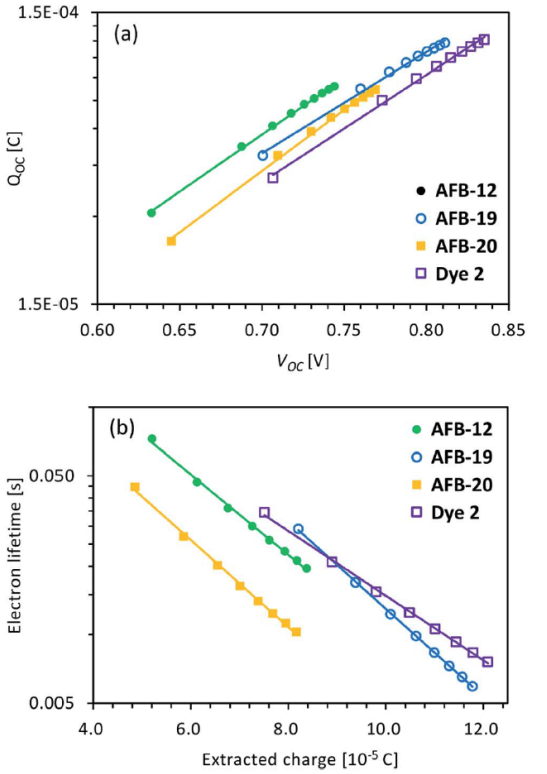

Fig. 9 (a) Charge extraction measurements at different light intensities and (b) electron lifetime measurements corrected for conduction band shift relative to AFB-12 in (a) and then plotted against the extracted charge for the same potentials.

interpret the observed V_{OC} shift to be predominantly caused by the conduction band shift and not by longer electron lifetimes.

The overall assessment of auxiliary donors for phenothiazine sensitizers is that they do provide only a moderate performance enhancement, through a slight increase in absorption and increased electron lifetimes. Because they are not in conjugation with the anchoring group, their contribution is limited to an inductive nature. In turn, this could be why the observed effects are only moderate. On the other hand, auxiliary donors could be used for tuning the properties not directly related to absorption, such as interactions with the redox couple, adjacent sensitizers or other electrolyte additives. If the use of copper or cobalt redox couples is desired for phenothiazine sensitizers, the synthetic efforts should be placed on tailoring the HOMO level, lowering the LUMO level and increasing the molar extinction coefficients.

Conclusions

In an attempt to understand the role of the auxiliary donor in phenothiazine sensitizers for DSSCs, we synthesized a series of dyes by varying only this moiety. Twelve sensitizers were evaluated, including ten different auxiliary donors, a reference sensitizer with no auxiliary donor and a "champion" phenothiazine dye (**Dye 2**).

The introduction of auxiliary donors marginally improved the absorption properties, raised the HOMO levels by up to 0.15 eV and improved the PCE by 4–11%, predominantly due to increased J_{SC} values. From electron lifetime and charge extraction measurements, it was also established that the addition of an auxiliary donor increased the electron lifetime by a factor of two. For the auxiliary donors, the efficiency followed the order phenyl < naphthyl < pyrene, with average PCEs of 4.76%, 4.90% and 5.00%. However, the overall performance differences between the auxiliary donors are within the limits of the standard deviations of the individual measurements. The effect of the chenodeoxycholic acid concentration in the staining solution for **AFB-19** revealed that a 10-fold molar excess was the most favorable concentration. The best device of the study was sensitized with **AFB-19**, delivering a photon-to-electron conversion efficiency of 5.36% with a $J_{SC} = 9.99$ mA cm^{-2}, $V_{OC} = 765$ mV and FF = 0.70.

The phenothiazine sensitizer with the highest reported PCE of 12.1% with an I^-/I_3^- electrolyte was also evaluated.[36] Although the dye had a high V_{OC}, the performance in terms of PCE was not significantly different from that of the other phenothiazine dyes in this study. Furthermore, integration of the published IPCE spectra implies that the PCE values reported by Nagarajan *et al.* are twice as high as theoretically possible under 1 sun AM 1.5G illumination. We therefore strongly encourage the practice of integrating the IPCE spectra and the use of reference sensitizers in this field.

Experimental section

Materials and reagents

Unless specifically mentioned, all reactions were performed under an inert atmosphere with chemicals used as received from Sigma Aldrich. The experimental procedure for the synthesis of the sensitizers can be found in the ESI.†

Characterization

NMR analyses (^{1}H and ^{13}C) were performed on either a Bruker 400 or 600 MHz spectrometer. Infrared absorption (IR) spectra were recorded on a Bruker Alpha FTIR spectrometer in attenuated total reflection (ATR) mode. UV/Vis spectra were recorded on a Hitachi U-1900 UV/Vis-spectrophotometer in quartz cuvettes with 10 mm light path. Fluorescence spectrophotometry was carried out on a Varian Cary Eclipse in quartz cuvettes. HRMS analysis was performed on a Waters Synapt G2-S Q-TOF instrument using either ASAP or ESI ionization.

Device fabrication

TEC-10 FTO glass sourced from Sigma Aldrich was washed with Deconex 21 solution (2 g L^{-1} H_2O) in an ultrasonic bath for 45 minutes before being rinsed with deionized water and ethanol. UV/O_3 cleaning for 15 minutes (Novascan PSD PRO-UV T6) was performed to remove organic contaminants from the FTO glass. A TiO_2 blocking layer was deposited by two hydrothermal depositions in 40 mM aqueous $TiCl_4$ solution at 70 °C for 30 minutes.

Two active layers of TiO_2 (18NR-T, GreatcellSolar) and one scattering layer (WER2-0, GreatcellSolar) were screen printed (mesh 53T, active area 0.238 cm^2) and then placed in a levelling chamber with ethanol for 3 minutes before drying on a hotplate for 6 minutes at 125 °C between each print. The electrodes were sintered in a programmable furnace (Nabertherm LT 9/12) with the ramping program of 125, 250, 325, 450, and 500 °C for 5, 5, 5, 15 and 15 minutes with 10 minutes ramping between each step. The total TiO_2 thickness was measured to be 16.5 μm (11 μm + 5.5 μm) using a profilometer (Veeco, Dektak 150). Finally, a post treatment in 40 mM aqueous $TiCl_4$ solution at 70 °C for 30 minutes was performed, followed by rinsing with deionized water and ethanol.

Platinum counter electrodes were fabricated from TEC-8 FTO glass (GreatcellSolar). Holes were drilled with a diamond drill bit, and a 10 mM H_2PtCl_6 platinum precursor solution in 2-propanol was drop-cast (5 μL cm^{-2}) onto the FTO and heated at 400 °C for 15 minutes. Prior to assembly, the counter electrodes were dried by a hot air gun at 400 °C for 25 minutes.

Due to varying indoor temperatures in Arctic Norway, staining of the electrodes was performed overnight in a 30 °C cabinet. Prior to staining the electrodes were annealed by a hot air gun at 480 °C for 25 minutes, and upon cooling to 80 °C they were immersed in the staining solutions. A dye concentration of 0.5 mM was used along with 10 equivalents of CDCA unless specified otherwise. N719 was stained using absolute ethanol while the organic dyes were stained using a mixture of acetonitrile and stabilized THF (43 : 57, v/v), which equates to a dielectric constant of 20, previously reported as the optimal value for dye staining.[54] After a staining time of 18 hours, the electrodes were rinsed with acetonitrile for 2 minutes before being sealed with the counter electrodes using a Surlyn gasket

(60 μm, Solaronix) in a drybox. Heating using a 50 W PTC heat element for 2 × 20 seconds provided efficient sealing.

The A6141 electrolyte contained 0.60 M 1-butyl-3-methylimidazolium iodide, 0.03 M I_2, 0.10 M guanidinium thiocyanate and 0.50 M *tert*-butylpyridine in a mixture of acetonitrile and valeronitrile (85 : 15, v/v).[6] The electrolyte was injected by vacuum backfilling before the hole was sealed with Surlyn and a circular glass cover disc. The electrodes were painted with conductive silver paint (Electrolube, SCP) before characterization.

Device characterization

J–V characteristics of the DSSCs were obtained under 1 sun AM 1.5G illumination from a Sciencetech SP300B solar simulator calibrated with a Newport Reference Cell (91150V), connected to a Keithley 2450 SourceMeter. The *J–V* scan rate was 12 mV s^{-1}, scanning from short-circuit to open-circuit. A circular mask with an aperture of 0.238 cm^2 was used for all *J–V* measurements. IPCE measurements were recorded from a device assembled using a halogen lamp (Ocean Optics HL-2000) and a monochromator (Spectral Products CM110) connected to the Keithley 2450 and programmed in LabView. The DSSCs and the NIST traceable calibrated photodiode (Thorlabs, FDS100-CAL) were masked with an aperture of 0.049 cm^2. Charge extraction and electron lifetime measurements were performed using a Dyenamo Toolbox. For the charge extraction measurements, the devices were illuminated using a white LED for 1 second at open circuit. When the light is switched off, the device is short-circuited and the extracted charge integrated. This is repeated for several light intensities by adjusting the LED bias from 50 to 450 mA in 50 mA increments. In the electron lifetime measurements, the LED light intensity was modulated, giving an AC response signal from the device from which the electron lifetimes were calculated.

Conflicts of interest

There are no conflicts to declare.

Acknowledgements

The authors would like to thank the Faculty of Natural Sciences and the Department of Chemistry at NTNU for financial support, Dr Susana Villa Gonzalez for HRMS analyses and Roger Aarvik for technical support. Associate professor Solon Economopoulos is thanked for helpful discussions on cyclic voltammetry, Sihai Luo for SEM imaging and Dr James Bannock for programming our IPCE setup. The Research Council of Norway is acknowledged for the support to the Norwegian Micro- and Nano-Fabrication Facility, NorFab (project number 245963/F50) and the Norwegian NMR Platform (project number 226244/F50).

References

1 B. O'Regan and M. Grätzel, *Nature*, 1991, **353**, 737–740.
2 M. Freitag, J. Teuscher, Y. Saygili, X. Zhang, F. Giordano, P. Liska, J. Hua, S. M. Zakeeruddin, J.-E. Moser, M. Grätzel and A. Hagfeldt, *Nat. Photonics*, 2017, **11**, 372–378.
3 O. Pekkola, C. Lungenschmied, P. Fejes, A. Handreck, W. Hermes, S. Irle, C. Lennartz, C. Schildknecht, P. Schillen, P. Schindler, R. Send, S. Valouch, E. Thiel and I. Bruder, *Sci. Rep.*, 2018, **8**, 9208.
4 A. Kay and M. Grätzel, *J. Phys. Chem.*, 1993, **97**, 6272–6277.
5 S. Cherian and C. C. Wamser, *J. Phys. Chem. B*, 2000, **104**, 3624–3629.
6 M. K. Nazeeruddin, F. De Angelis, S. Fantacci, A. Selloni, G. Viscardi, P. Liska, S. Ito, B. Takeru and M. Grätzel, *J. Am. Chem. Soc.*, 2005, **127**, 16835–16847.
7 T. Horiuchi, H. Miura, K. Sumioka and S. Uchida, *J. Am. Chem. Soc.*, 2004, **126**, 12218–12219.
8 A. Hagfeldt, G. Boschloo, L. Sun, L. Kloo and H. Pettersson, *Chem. Rev.*, 2010, **110**, 6595–6663.
9 N. Robertson, *Angew. Chem., Int. Ed.*, 2006, **45**, 2338–2345.
10 A. Mishra, M. K. Fischer and P. Bäuerle, *Angew. Chem., Int. Ed.*, 2009, **48**, 2474–2499.
11 M. Pazoki, U. B. Cappel, E. M. J. Johansson, A. Hagfeldt and G. Boschloo, *Energy Environ. Sci.*, 2017, **10**, 672–709.
12 Y. Hu, A. Abate, Y. Cao, A. Ivaturi, S. M. Zakeeruddin, M. Grätzel and N. Robertson, *J. Phys. Chem. C*, 2016, **120**, 15027–15034.
13 Y. Hu, A. Ivaturi, M. Planells, C. L. Boldrini, A. O. Biroli and N. Robertson, *J. Mater. Chem. C*, 2016, **4**, 2509–2516.
14 L. Zhang and J. M. Cole, *ACS Appl. Mater. Interfaces*, 2015, **7**, 3427–3455.
15 D. Joly, L. Pellejà, S. Narbey, F. Oswald, J. Chiron, J. N. Clifford, E. Palomares and R. Demadrille, *Sci. Rep.*, 2014, **4**, 4033.
16 S. H. Kim, H. W. Kim, C. Sakong, J. Namgoong, S. W. Park, M. J. Ko, C. H. Lee, W. I. Lee and J. P. Kim, *Org. Lett.*, 2011, **13**, 5784–5787.
17 H. N. Tsao, C. Yi, T. Moehl, J.-H. Yum, S. M. Zakeeruddin, M. K. Nazeeruddin and M. Grätzel, *ChemSusChem*, 2011, **4**, 591–594.
18 A. Mahmood, *Sol. Energy*, 2016, **123**, 127–144.
19 Z.-S. Huang, H. Meier and D. Cao, *J. Mater. Chem. C*, 2016, **4**, 2404–2426.
20 R. Y.-Y. Lin, F.-L. Wu, C.-T. Li, P.-Y. Chen, K.-C. Ho and J. T. Lin, *ChemSusChem*, 2015, **8**, 2503–2513.
21 K. D. Seo, H. M. Song, M. J. Lee, M. Pastore, C. Anselmi, F. De Angelis, M. K. Nazeeruddin, M. Grätzel and H. K. Kim, *Dyes Pigm.*, 2011, **90**, 304–310.
22 A. Venkateswararao and K. R. J. Thomas, in *Solar Cell Nanotechnology*, 2013, pp. 41–96.
23 Y. Hua, S. Chang, D. D. Huang, X. Zhou, X. J. Zhu, J. Z. Zhao, T. Chen, W. Y. Wong and W. K. Wong, *Chem. Mater.*, 2013, **25**, 2146–2153.
24 H.-H. Gao, X. Qian, W.-Y. Chang, S.-S. Wang, Y.-Z. Zhu and J.-Y. Zheng, *J. Power Sources*, 2016, **307**, 866–874.
25 X. Yang, J. Zhao, L. Wang, J. Tian and L. Sun, *RSC Adv.*, 2014, **4**, 24377–24383.
26 W. Wu, J. Yang, J. Hua, J. Tang, L. Zhang, Y. Long and H. Tian, *J. Mater. Chem.*, 2010, **20**, 1772–1779.

27 J. Li, W. Wu, J. Yang, J. Tang, Y. Long and J. Hua, *Sci. China: Chem.*, 2011, **54**, 699–706.
28 D. Muenmart, N. Prachumrak, R. Tarsang, S. Namungruk, S. Jungsuttiwong, T. Sudyoadsuk, P. Pattanasattayavong and V. Promarak, *RSC Adv.*, 2016, **6**, 38481–38493.
29 X. Zhang, F. Gou, J. Shi, H. Gao, C. Xu, Z. Zhu and H. Jing, *RSC Adv.*, 2016, **6**, 106380–106386.
30 S. Wang, H. Wang, J. Guo, H. Tang and J. Zhao, *Dyes Pigm.*, 2014, **109**, 96–104.
31 E. Mosconi, J.-H. Yum, F. Kessler, C. J. Gómez García, C. Zuccaccia, A. Cinti, M. K. Nazeeruddin, M. Grätzel and F. De Angelis, *J. Am. Chem. Soc.*, 2012, **134**, 19438–19453.
32 P. Gao, Y. J. Kim, J.-H. Yum, T. W. Holcombe, M. K. Nazeeruddin and M. Grätzel, *J. Mater. Chem. A*, 2013, **1**, 5535–5544.
33 S. M. Feldt, E. A. Gibson, E. Gabrielsson, L. Sun, G. Boschloo and A. Hagfeldt, *J. Am. Chem. Soc.*, 2010, **132**, 16714–16724.
34 Y. S. Yang, H. D. Kim, J.-H. Ryu, K. K. Kim, S. S. Park, K.-S. Ahn and J. H. Kim, *Synth. Met.*, 2011, **161**, 850–855.
35 H. Wei, J. Shen, Y. Liu, T. Huang, Q. Zhang, J. Zhao and X. Zhao, *Dyes Pigm.*, 2018, **149**, 789–795.
36 B. Nagarajan, S. Kushwaha, R. Elumalai, S. Mandal, K. Ramanujam and D. Raghavachari, *J. Mater. Chem. A*, 2017, **5**, 10289–10300.
37 A. F. Buene, N. Uggerud, S. P. Economopoulos, O. R. Gautun and B. H. Hoff, *Dyes Pigm.*, 2018, **151**, 263–271.
38 R. Y.-Y. Lin, T.-M. Chuang, F.-L. Wu, P.-Y. Chen, T.-C. Chu, J.-S. Ni, M.-S. Fan, Y.-H. Lo, K.-C. Ho and J. T. Lin, *ChemSusChem*, 2015, **8**, 105–113.
39 N. S. Wilson and B. A. Keay, *Tetrahedron Lett.*, 1996, **37**, 153–156.
40 N. S. Wilson and B. A. Keay, *Tetrahedron Lett.*, 1997, **38**, 187–190.
41 K. L. Billingsley and S. L. Buchwald, *J. Org. Chem.*, 2008, **73**, 5589–5591.
42 Z. Iqbal, W.-Q. Wu, Z.-S. Huang, L. Wang, D.-B. Kuang, H. Meier and D. Cao, *Dyes Pigm.*, 2016, **124**, 63–71.
43 J. Chen, Y. Zhang, L. Yang, X. Zhang, J. Liu, L. Li and H. Zhang, *Tetrahedron*, 2007, **63**, 4266–4270.
44 H. Svith, H. Jensen, J. Almstedt, P. Andersson, T. Lundbäck, K. Daasbjerg and M. Jonsson, *J. Phys. Chem. A*, 2004, **108**, 4805–4811.
45 G. Boschloo and A. Hagfeldt, *Acc. Chem. Res.*, 2009, **42**, 1819–1826.
46 H. J. Snaith, *Adv. Funct. Mater.*, 2010, **20**, 13–19.
47 J. A. Christians, J. S. Manser and P. V. Kamat, *J. Phys. Chem. Lett.*, 2015, **6**, 852–857.
48 H. Ellis, N. Vlachopoulos, L. Häggman, C. Perruchot, M. Jouini, G. Boschloo and A. Hagfeldt, *Electrochim. Acta*, 2013, **107**, 45–51.
49 Y. Saygili, M. Söderberg, N. Pellet, F. Giordano, Y. Cao, A. B. Muñoz-García, S. M. Zakeeruddin, N. Vlachopoulos, M. Pavone, G. Boschloo, L. Kavan, J.-E. Moser, M. Grätzel, A. Hagfeldt and M. Freitag, *J. Am. Chem. Soc.*, 2016, **138**, 15087–15096.
50 P. Ferdowsi, Y. Saygili, S. M. Zakeeruddin, J. Mokhtari, M. Grätzel, A. Hagfeldt and L. Kavan, *Electrochim. Acta*, 2018, **265**, 194–201.
51 R. M. El-Shishtawy, J.-D. Decoppet, F. A. M. Al-Zahrani, Y. Cao, S. B. Khan, M. S. Al-Ghamdi, B. G. Alhogbi, A. M. Asiri, S. M. Zakeeruddin and M. Grätzel, *New J. Chem.*, 2018, **42**, 9045–9050.
52 R. Flamholc, D. Plażuk, J. Zakrzewski, R. Métivier, K. Nakatani, A. Makal and K. Woźniak, *RSC Adv.*, 2014, **4**, 31594–31601.
53 Y. Hao, H. Tian, J. Cong, W. Yang, I. Bora, L. Sun, G. Boschloo and A. Hagfeldt, *ChemPhysChem*, 2014, **15**, 3476–3483.
54 H. Ozawa, M. Awa, T. Ono and H. Arakawa, *Chem.–Asian J.*, 2012, **7**, 156–162.